EUROPEAN ORGANIZATION FOR NUCLEAR RESEARCH

CERN/EF 88-11
8 August 1988

FORWARD CALORIMETRY IN THE UPGRADED UA1 EXPERIMENT

UA1 Collaboration

Aachen[1]-Amsterdam (NIKHEF)[2]-Annecy (LAPP)[3]-Birmingham[4]-CERN[5]-
Harvard[6]-Helsinki[7]-Kiel[8]-Imperial College, London[9]-
Queen Mary College, London[10]-Madrid (CIEMAT)[11]-MIT[12]-Padua[13]-
Paris (CdF)[14]-Riverside[15]-Roma[16]-Rutherford Appleton Lab.[17]-
Saclay (CEN)[18]-UCLA[19] and Vienna[20]

F.J. Alvarez-Taviel[11], C. Bacci[16], F. Diez-Hedo[11], P. Doncel[11],
A. Ferrando[5,11], A. Givernaud[5,18], M.A. Marquina[11], E. Petrolo[16],
T. Rodrigo[11], C. Rubbia[5], A. Tusi[16] and V. Vuillemin[5]

ABSTRACT

The major improvement in the upgraded UA1 calorimetry at the $S\bar{p}pS$ is the general use of ionization chambers filled with Tetramethylpentane (TMP) as a detection medium interspersed with uranium (U) plates as absorber. To achieve overall uniformity of detection down to very small angles, an identical solution is proposed for the Forward Calorimetry. Forward calorimetry is essential for good total and missing energy measurement at high luminosity in view of the increasing rate of multiple collisions. Both designs for ForWard (FW) and Very ForWard (VFW) calorimeters are presented along with expected resolutions.

Presented at the International Conference on Advanced Technology and Particle Physics, Centro di Cultura Scientifica A. Volta, Villa Olmo, Como, Italy, 13-17 June 1988

[Proceedings published by Nucl. Instr. & Methods]

EF/4011F/VV/ef

1. INTRODUCTION

One of the goals of the upgraded UA1 detector [1] will be to profit from the high luminosities to be achieved with the new $\bar{p}$ accumulator AA/ACOL at the CERN $\bar{p}$ Collider. Among the crucial aims of the UA1 Experiment are the improvement on the missing energy resolution as well as the measurement of the total energy contained in single or multiple collisions [2]. A calorimetry with full solid angle coverage for best missing-energy measurement is essential for instance for any search of new type of particles, giving a relatively large amount of missing energy, such as top quark or supersymmetric particles. A better determination of the mass of the W and better estimate of its longitudinal momentum are also among the new desirable improvements [3]. The separation between single and multiple interactions becomes more and more important as the luminosity increases and a good determination of the total energy is the only powerful mean available to deal with this problem.

In order to achieve these goals, all new calorimeters in UA1 are made of U plates as absorber, for good energy measurement given the constraints of the predefined and limited space available in the existing apparatus, and for improved electron/pion compensation essential to the measurement of the correct jet energy. The active medium intermixed with the U plates is provided by compact ionization boxes filled with a liquid used at room temperature giving a high yield of free electrons, the Tetramethylpentane (TMP) [4]. The design guarantees also the best possible granularity achieved using small detection elements arranged according to a tower structure.

This paper is organized as follows: in sect. 2, some generalities are developped concerning FW calorimetry in the specific context of the UA1 Experiment, sect. 3 gives details of the design of the FW calorimeter, sect. 4 deals with the design of the VFW calorimeter. The question of fine segmentation in radius-azimuth and in depth is discussed in sect. 5 as well as few expected performances.

2. FORWARD CALORIMETRY IN UA1

Fig. 1 shows an overall view of the UA1 Experiment. The FW calorimetry consists of a two-arm spectrometer, each arm being made of two distinct calorimeters [5]:

- FW: a ForWard calorimeter, situated into the octogonal hole of the hadronic endcaps;

- VFW: a Very ForWard calorimeter, situated further away between the compensating magnet of the main dipole and the last focusing quadrupole of the SPS straight section.

Dimensions of the vacuum beam pipe have been kept minimal in those two regions to approach the beam line as much as allowed by the size of the beam profile in order to collect the largest amount of energy with these calorimeters. In the VFW region the beam pipe has an elliptical shape, 65 mm x 75 mm, slightly superior to the limiting aperture of the SPS Collider. In both cases FW and VFW calorimeters placement is fixed and the length in depth is on the order of 1.1 m, which ultimately limits the number of interaction lengths to 6 units. Given this fixed space, any other absorbing medium would provide less interaction lengths for an identical segmentation which is certainly not desirable given the high energy of the particles produced in the fragmentation region. The solid-angle coverage of the two calorimeters is indicated in table 1. With a pseudo-rapidity range between 4.5 and 6.5, the VFW calorimeters are well matched to select single diffractive processes by requiring energy imbalance between both sides [6].

The sharing of energies between the new calorimeters is indicated in table 2 for different topologies of events generated by ISAJET, version 5.25 [7] and simulating the new detector set-up. It shows the importance of the FW and VFW calorimeters in total energy measurement.

The choice of U-TMP stacks for FW and VFW calorimeters, in addition to its intrinsic advantages, is justified by the desirable uniformity of the detection all around the available solid angle. It should be pointed out anyway that scintillators would not be a judicious choice due to the amount of radiation in these forward regions, close to beam line. Standardization of readouts for all detectors is then also an obvious advantage.

3. THE FW CALORIMETER

The FW calorimeter is located in the middle octogonal hole of the hadronic endcaps (called I's). The I's are built in two halves, one is fixed as it supports the central drift chambers and the beam pipe, and the other one is movable for easy access. If one considers all together the problems of TMP filling, stacks of TMP boxes and U, easy installation in situ, manageable weight of the units and so on, one

realizes all the advantages of a modular design for the FW calorimeter. The design should then ensure that the losses in the vertical plane in between the two halves of the different calorimeter modules are minimal when both I's are closed in order to obtain the best possible hermeticity in the forward direction.

According to these considerations, the FW calorimeter consists on each side of the interaction region of 12 half–octogonal prisms, 6 attached to the fixed I, and 6 to the movable one. Once the I's are closed, the distance between both halves of the detector will be on the order of 2–3 mm, leaving a central hole (120 mm diameter) in order to fit the beam pipe in (83 mm internal diameter, 1.5 mm thick). Each pair of half–prisms constitute a module of the FW calorimeter (fig. 2). All modules are identical and made of sandwiches of 10 TMP boxes intersperced with 10 mm U absorber (made of 2 x 5 mm U plates). The supporting plates on each side of the modules are made in Anticorrodal™ (15 mm thickness). The overall weight of each module is around 250 kg. A summary of all characteristics of the FW calorimeter and modules is given in table 3. In order to have the maximal azimuthal coverage and minimize all losses due to gaps in between the boxes containing the TMP liquid, we choose to build each TMP box in one single structure. TMP boxes would then have a half–octogonal shape, as shown in fig. 3.

On the practical side, this design brings several difficulties [8]:

- the skeleton of the box made of low–carbon stainless steel bars is of a non–trivial shape;
- the HV/signal connection between the internal electrodes and the HV feedthroughs situated at the periphery of the box cannot be direct, they will have to be interconnected via insulated wires for example, without polluting the TMP liquid.

Fig. 3 shows the skeleton structure of a TMP box made out of a $3 \times 3\ mm^2$ section stainless steel bar. Four separate sections are foreseen to receive 2 electrodes each. The 3 separation bars are pierced to allow the filling of the 4 compartments with TMP. The position of the holes (2.2 mm diameter) for the feedthroughs and the filling pipe can be seen at the outer part of the frame. The electrodes are of two different types, which are required to have a trapezoidal shape. Their dimensions are given in table 4 along with the expected noise over signal ratio given the capacitances of the electrodes and front–end readout. The feeding is done by standard feedthroughs. In the case of the inner electrodes, the HV is driven with thin wires passing through ceramic tubes.

Two goals were considered in designing the granularity of the FW calorimeter: minimization of the multiple hits on the electrodes and best overall resolution in missing E_T. Giving the complicated geometry of the TMP boxes, the idea of special position detectors was in first approximation discarded. On the other hand, the radial development of the showers in U is quite narrow. More than 90% of the energy is contained in a few centimetres diameter [9]. Then, of course, a finer structure than the present one would ensure a shower separation in most cases.

However, the adopted solution represents a compromise between a too complicate design with multiple electrodes and a single electrode per compartment design, where the E_T information would be lost.

4. THE VFW CALORIMETER

The VFW calorimeter is of a more conventional geometry. Each side is made of 4 double independent modules arranged as a mosaic around the beam pipe as seen in fig. 4. Its vertical dimension is bigger than the horizontal one in order to detect all forward particles after the vertical deflection of the compensating coil situated between the interaction region and the VFW calorimeter. Each quarter of the VFW detector has 60 stacks (10 mm U and TMP boxes) representing around 6 interaction lengths.

The TMP boxes are of two different dimensions. An example is given in fig. 5. Two separate sections with 4 electrodes each are joined by an intermediate bar pierced of several holes to allow the TMP liquid to fill in the entire box. All HV feedthroughs are directly connected to the electrodes and welded in the 3×3 mm^2 stainless steel frame. Sizes, average capacitances of electrodes and expected signal over noise ratio are indicated in table 4. The conception of all VFW TMP boxes is very similar to the one developped first for the central calorimeter. All parameters of the VFW calorimeter are listed in table 5.

5. SEGMENTATION AND EXPECTED PERFORMANCES

The physical total space available for the TMP boxes and U absorber of the FW and VFW calorimeters is fixed, given by the existing geometry of the UA1 Experiment, and in the order of 1.1 m in depth in both cases. The number of boxes possible is then directly related to the width of passive material. Several geometrical

scenarios have been simulated [9]. For each of the various configurations, showers were generated via GEANT, version 3.11 [10]. Only completely contained showers were used in the present study for the calculation of resolutions. A good description of the method can be found in ref. [11] and will not be discussed here.

The following geometries have been studied:

- 120 stacks, 5 mm U plates, 3.3 mm TMP boxes, 5.7 γ_I ;
- 75 stacks, 10 mm U plates, 3.3 mm TMP boxes, 7.1 γ_I ;
- 55 stacks, 15 mm U plates, 3.3 mm TMP boxes, 7.9 γ_I ;
- 43 stacks, 20 mm U plates, 3.3 mm TMP boxes, 8.2 γ_I .

For both electron and pion showers, the energy resolution is computed from the distribution of the total energy collection and that for the various geometries and incident electrons from 2 to 100 GeV, pions from 10 to 100 GeV. All these distributions show a gaussian shape. The widths (σ) are directly related to the resolutions, R, by

$$\sigma/E = R(\%)/\sqrt{E} \ .$$

5.1 Electrons

For electrons, the corresponding resolutions are given in fig. 6(a). The lines correspond to the averages weighted by errors. The resolution, R, is independent of the energy in all cases. For a given material the resolution appears to be linear with the thickness. For the U it can be parametrized as

$$R_e(\%) = \sigma/E * \sqrt{E} = (2.12 \pm 0.06) * t(mm) + (9.13 \pm 0.63) \ .$$

In comparison with the 5 mm U-plates option, the 15 mm U-plates case is 100% worse and the 10 mm U deteriorates the energy resolution by 50%. Then, 5 and 10 mm U are the best choices with the results

$\sigma/E = 20\%/\sqrt{E}$, 5 mm U plates,
$\sigma/E = 31\%/\sqrt{E}$, 10 mm U plates.

5.2 Pions

For pions one notices the appearance of a term depending on the energy as shown in fig. 6(b). The error on the energy does not follow the same formula but is now described by an expression of the form

$$\sigma/E = R_h(\%)/\sqrt{E} + b(\%) \ .$$

R_h values are 50%, 69% and 80% respectively, for the three U plates types. Notice that R_h/R_e is ~ 2 for all thicknesses. The constant term varies from 0.9% to 2.4%, increasing almost linearly with the thickness. Similar effects have been already pointed out in the litterature [12]. In function of the U-plates thickness, the resolution follows a degradation

$$R_h(\%) = (0.26 \pm 0.08)\sqrt{t(mm)} + (0.01 \pm 0.02) .$$

5.3 The e/π ratio

Discussions on compensation for different active and passive materials can be found in refs [12] and [13], and on U and Pb in ref. [14]. In our case, one of the biggest constraints is the unknown Birk's factor for TMP. We have used $k_B = 0.014$ cm/MeV in the present study, obtaining the results shown in fig. 7 [15].

The ratios for the various plates are constant with the energy, being

$$\begin{aligned} e/\pi \text{ ratio} = \quad & 0.906 \pm 0.006, \text{ 5 mm U} , \\ & 0.834 \pm 0.005, \text{ 10 mm U} , \\ & 0.808 \pm 0.004, \text{ 15 mm U} . \end{aligned}$$

5.4 The single/multiple collision separation problem

For the 5 and 10 mm U geometries, 1000 events of the type minimum bias and two jets ($p_j^T \geqq 50$ GeV) were generated and simulated through the complete detector, using the resolutions found for the electromagnetic and hadronic energies in the FW and VFW calorimeters. Fig. 8(a) shows the dN/dE distribution per event (MB) for the 10 mm geometries. The shapes of the distributions for 5 mm and 10 mm U do not differ too much. The average collected energy per event is 403.3 GeV. The fraction of events having a total energy collected in the UA1 apparatus bigger than 80% $\sqrt{s}$ is 26%. Similar picture is observed looking at the two-jet (TJ) events, as shown in fig. 8(b). In this case the average collected energy per event is larger and equal to 539.4 GeV and the fraction of events of which the total energy collected is bigger than 80% $\sqrt{s}$ is 81%.

Concerning the single/double collision separation in case of MB events, a cut on $E < 630$ GeV separates the two topologies with an efficiency of ~ 90.6% in the 10 mm U case. In the case of high p_T events TJ combined with an underlying MB collision, the separation efficiency between single and double collisions is quite high: ~ 96.9% for the 10 mm U case.

5.5 Missing E_T resolution

With the FW calorimeter the missing transverse energy resolution reaches the value

$$\sigma \text{ (missing } E_T)/E_T = \sim 0.4/\sqrt{E_T} \text{ ,}$$

where E_T is the total scalar sum of transverse energies. In addition to the 2 electrodes in radius, as shown in fig. 9, the cases of 4 and 1 electrodes have been considered. The difference between 2 and 4 cells in radius is quite small, the improvement is inside the statistical errors (2 to 3%). For the one-electrode case, of course, the FW calorimeter is not able to provide any estimate for missing E_T.

Concerning electronic readout, there are twelve readout samplings in depth after ganging together five electrodes in the direction parallel to the beam (fig. 10). In r-ϕ orientation, each module contains 8 electrodes, so each plane contains 16 electrodes around the beam line. The overall number of readout channels is then: (2 sides) x (16 electrodes/plane) x (12 samplings in depth) = 384 channels. These are multiplexed and digitized by the standard electronics developped for all upgraded calorimeters in UA1 [16].

6. SUMMARY AND CONCLUSIONS

The present design of the overall FW calorimetry, coming down to 3 mrad, being of a good compacticity, and negligible cracks between modules, will convert UA1 in the most hermetic of all major $\bar{p}p$ detectors.

The major novelty compared to Central Calorimetry is the real complexity of the forward TMP boxes, with all the feedthroughs on the same frame side. That allows to minimize the unwanted energy losses through gaps in the detectors. The optimization in the number of U plates and readout channels reduces considerably the total cost. We are able to propose a set-up having excellent performances:

- good geometrical acceptance;
- performant in total energy collection, allowing single/multiple interactions to be separated;
- improvement in the missing E_T resolution, and
- triggering capabilities in the forward region.

Acknowledgements

We are thankful to the management and staff of CERN and of all participating institutes for their vigourous support of the project. The following funding agencies have contributed to this program:

CIEMAT, Madrid, Spain,
Istituto Nazionale di Fisica Nucleare (INFN), Italy.

We acknowledge very useful discussions, advices and help from M. Aguilar-Benitez, A. Bézaguet, M. Daniel, L. Dumps, A. Gonidec, J.L. Gutierrez, J.M. Martinez, G. Maurin, L. Naumann, A. Placci, E. Radermacher and D. Schinzel.

REFERENCES

[1] C. Rubbia, UA1 improvement programme: A status report for the SPSC, unpublished (1988);
UA1 Collaboration, Design report of a U-TMP calorimeter for the UA1 Experiment with ACOL, R37 UA-1 (1986);
J. Dowell, preprint CERN/EP 86-193 (1986);
M. Albrow et al., Nucl. Instr. and Meth. A265 (1988) 303-318.

[2] A. Ferrando et al., UA1 Technical Note TN/87-70 (1987).

[3] A. Ferrando et al., UA1 Technical Note TN/87-91 (1987).

[4] A. Gonidec et al., preprint CERN/EP 88-36, submitted to Nucl. Instr. and Methods (1988).

[5] F.J. Alvarez-Taviel et al., UA1 Technical Note TN/87-10 (1987).

[6] M.G. Albrow et al., UA1 Technical Note TN/87-90 (1987).

[7] F. Paige and S. Protopopescu, ISAJET version 5.25, BNL 29777 (1981).

[8] F.J. Alvarez-Taviel et al., UA1 Technical Note TN/88-22 (1988).

[9] F. Diez-Hedo et al., UA1 Technical Note TN/88-16 (1988).

[10] GEANT3 User's Guide, CERN/DD/EE 84-1, September 1987.

[11] A. Givernaud, UA1 Technical Note TN/86-109 (1986).

[12] M. De Vicenzi et al., preprint CERN/EP 85-126, 12 August 1985;
M. De Vicenzi et al., preprint CERN/EP 86-12, 31 January 1986;
R. Wigmans, preprint CERN/EF 86-18 (1986).

[13] V. Bohmer et al., Nucl. Instr. and Meth. 122 (1974) 313;
J. Engler et al., Nucl. Instr. and Meth. 106 (1973) 189.

[14] C.W. Fabjan et al., Nucl. Instr. and Meth. 141 (1977) 61;
C.W. Fabjan, preprint CERN/EP 86-45, 4 April 1986.

[15] B. Aubert et al., UA1 Technical Note TN/87-89 (1987).

[16] C. Bacci et al., UA1 Technical Note TN/88-08, submitted to Nucl. Instr. and Methods (1988).

TABLE CAPTIONS

Table 1 Solid angle coverage and pseudorapidity range of the forward calorimeters.

Table 2 Sharing of collected energies in the different upgraded calorimeters for minimum bias events, 2-jets, Single Diffractive (SD) and Double Diffractive (DD) events.

Table 3 Summary of parameters of the FW calorimeter.

Table 4 Sizes of electrodes, capacitances and expected electronic signal/noise ratio for the FW and VFW calorimeters.

Table 5 Summary of parameters of the VFW calorimeter.

TABLE 1

	Forward calorimeter	Very forward calorimeter
Distance to interaction point	4 m	12.4 m
Minimum radius	60 mm	35 mm
Maximum radius	300 mm	270 mm
Polar angle range	15 – 75 mrad	2.8 – 21.8 mrad
Pseudorapidity range	3.3 – 4.9	4.5 – 6.5

TABLE 2

	Min. bias	2-jets	SD	DD
Central calorimeters	12 GeV	115 GeV	~ 0	~ 0
Endcap calorimeters	85 GeV	115 GeV	18 GeV	~ 0
Forward calorimeters	106 GeV	169 GeV	50 GeV 1 side only	~ 0
Very forward calorimeters	200 GeV	100 GeV	110 GeV 1 side only	~ 120 GeV
Total	403 GeV	539 GeV		

TABLE 3

(a) Specifications of the FW calorimeter

Number of modules	24
	4 (quarters of 6 modules each)
Number of TMP boxes	240
Number of U plates	432 (5 mm thickness)
Number of electrodes	1920
Number of readout channels	384
Number of litres TMP	80 ℓ

(b) Specifications of the forward/backward side

Depth	918 mm
Inner size radius	60 mm
Outer size radius	300 mm
Total weight	3 t
Segmentation	8 cells in ϕ
	2 cells in R
	12 samplings in depth
Number of inter. lenghts	6

(c) Specifications of each module

Number of TMP boxes	10
U plates thickness	10 mm (2 x 5 mm)
Number of U plates	9 (of 10 mm, 18 x 5 mm plates)
Length	153 mm
Weight	250 kg
End-plates	Aluminium (15 mm thickness)

TABLE 4

(a) Specifications of the VFW calorimeter

Number of modules	16 2 sides of 8 modules each
Number of TMP boxes	480
Number of U plates	928 (5 mm thickness)
Number of electrodes	3968
Number of readout channels	768
Number of litres TMP	180 ℓ

(b) Specifications of the forward/backward side

Depth	865 mm
Inner size radius	~ 68 x 78 mm^2
Outer size radius	~ 1037 mm x 555 mm
Total weight	6.6 t
Segmentation	x – y 32 electrodes/plane 12 samplings in depth
Number of inter. lenghts	6.2

(c) Specifications of each module

Number of TMP boxes	30
U plates thickness	10 mm (2 x 5 mm)
Number of U plates	29 (of 10 mm, 58 x 5 mm plates)
Length	419 mm
Weight	831 kg
End-plates	Aluminium (15 mm thickness)

TABLE 5

SIZES AND CAPACITANCES OF ELECTRODES
(computed on the basis of 340 pF for 100 cm^2)

Forward calorimeter:

Electrode	h [mm]	Widths [mm]	[mm]	S [cm^2]	C [pF]
Internal	103	44	130	89.6	304.7
External	103	127	212	174.6	593.6

Very forward calorimeter:

Electrode	h [mm]	Width [mm]	S [cm^2]	C [pF]
Average size	139	114	152	537

SIGNAL OVER ELECTRONIC NOISE RATIOS

Forward calorimeter:

Number of layers/sampling	Electrode	C [nF]	q_{MIP} [ref.]	ENC [ref.]	S/N (q_{MIP})
5	int.	1.52	22 720	2628	8.6
	ext.	2.97		4325	5.3

Very forward calorimeter:

Number of layers/sampling	Electrode	C [nF]	q_{MIP} [ref.]	ENC [ref.]	S/N (q_{MIP})
5	Average size	2.7	22 720	4000	5.7

FIGURE CAPTIONS

Fig. 1 Overall view of the UA1 Experiment showing the four FW calorimeters.

Fig. 2 View of a plane of the FW calorimeter with its support system inside the hadronic endcaps. Each plane contains two stainless steel boxes of a half-octogonal shape.

Fig. 3 Drawing of a TMP box for the FW calorimeter showing all parts: the stainless steel frame with three intermediate bars, the eight electrodes, ceramic pieces, HV feedthroughs and TMP tubes.

Fig. 4 View of the VFW calorimeter.

Fig. 5 Drawing of a TMP box for the VFW calorimeter showing all parts: the stainless steel frame with the intermediate bar, the eight electrodes, HV feedthroughs and TMP tubes.

Fig. 6 Resolutions as a function of different incident energies: (a) electromagnetic resolution and (b) hadronic resolution.

Fig. 7 e/π ratio as a function of energy.

Fig. 8 Total energy distribution for 10 mm U plates: (a) minimum bias and (b) two-jets.

Fig. 9 σ_T/E_T distribution, as a function of E_T and resolution function fit.

Fig. 10 Schematic of one quarter of the FW calorimeter showing the six modules, each of them containing U plates and 10 TMP boxes.

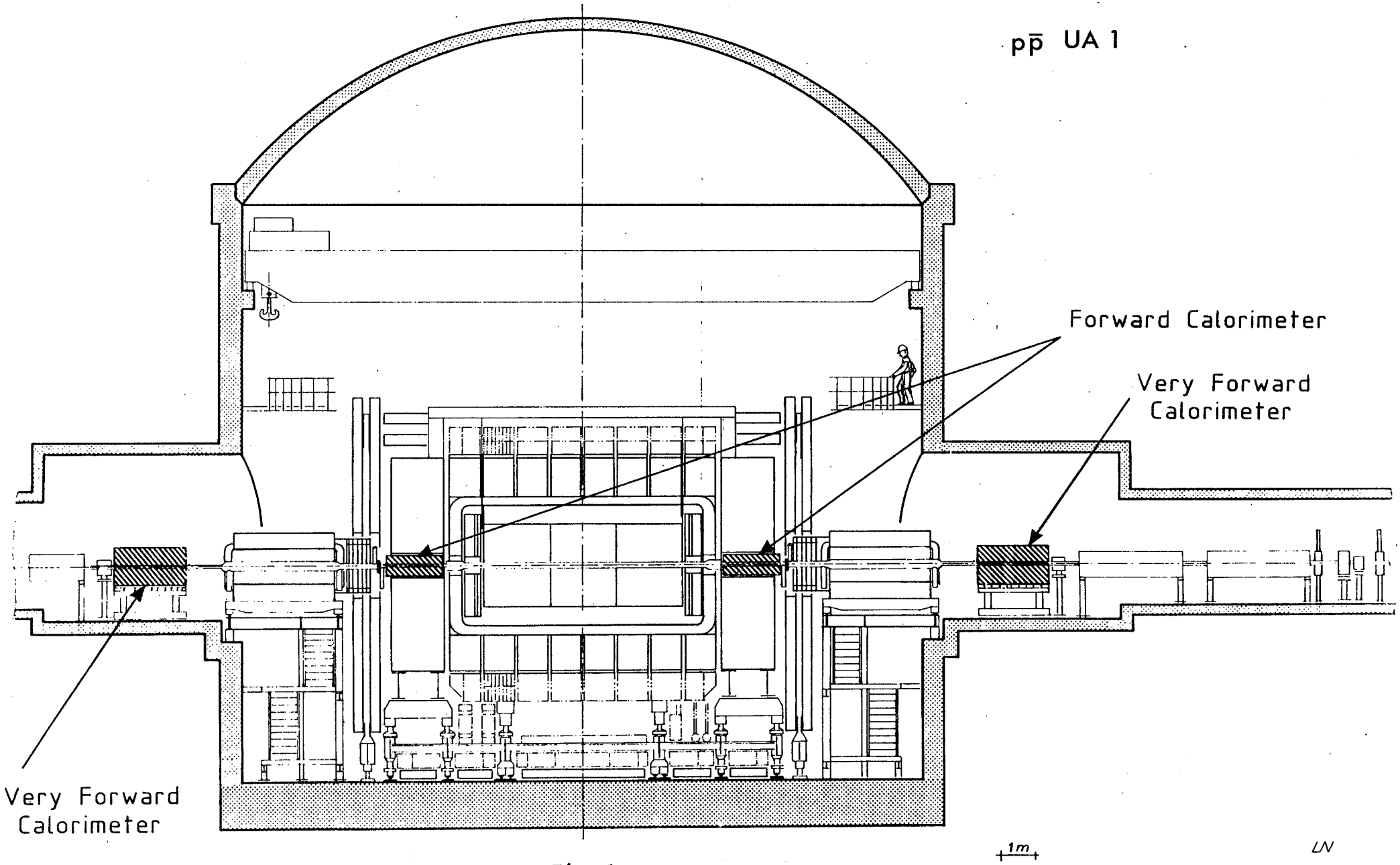
pp̄ UA 1
Forward Calorimeter
Very Forward Calorimeter
Very Forward Calorimeter
1m
LN

Fig. 1

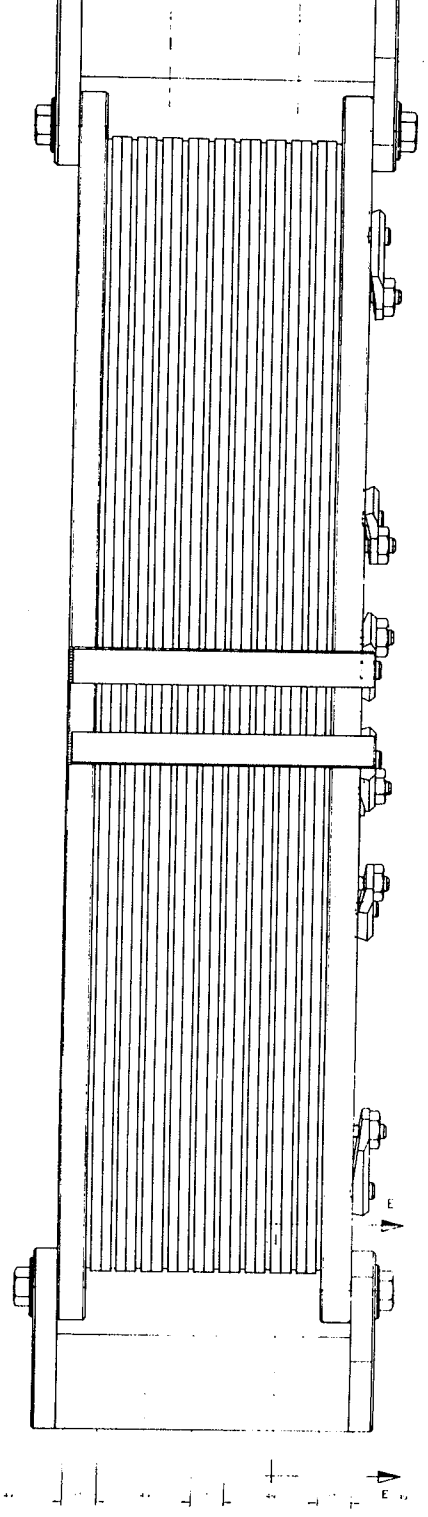

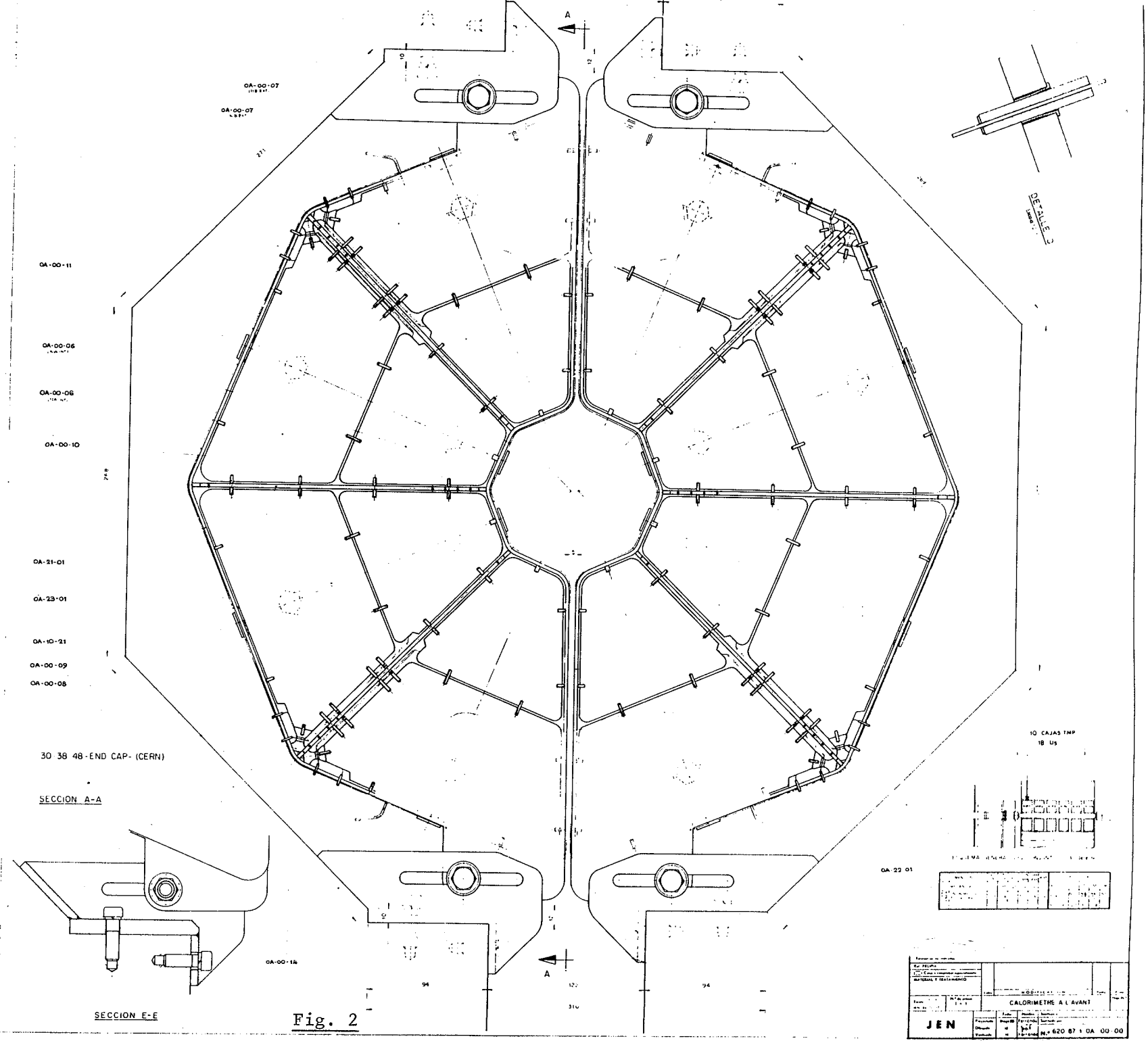
0A-00-07
0A-00-07
0A-00-11
0A-00-06
0A-00-06
0A-00-10
0A-21-01
0A-23-01
0A-10-21
0A-00-09
0A-00-08
30 38 48-END CAP- (CERN)
SECCION A-A
SECCION E-E
0A-00-14
DETALLE C
10 CAJAS TMP
18 Us
0A-22-01
CALORIMETRE A L'AVANT
JEN
N.º 620 87 1 0A 00 00

Fig. 2

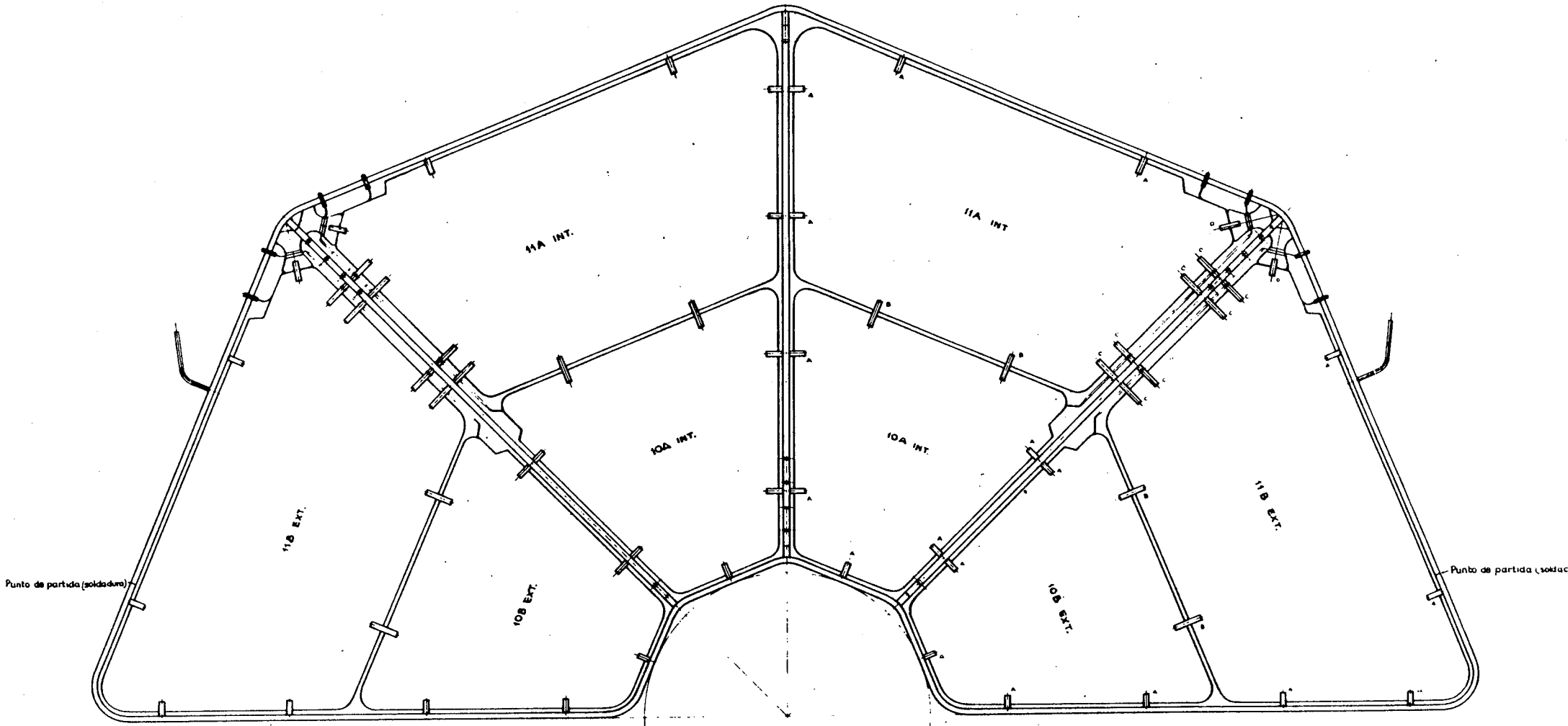
11A INT.
11A INT
10A INT.
10A INT
11B EXT.
10B EXT.
10B EXT.
11B EXT.
Punto de partida (soldadura)
Punto de partida (soldad

Fig. 3

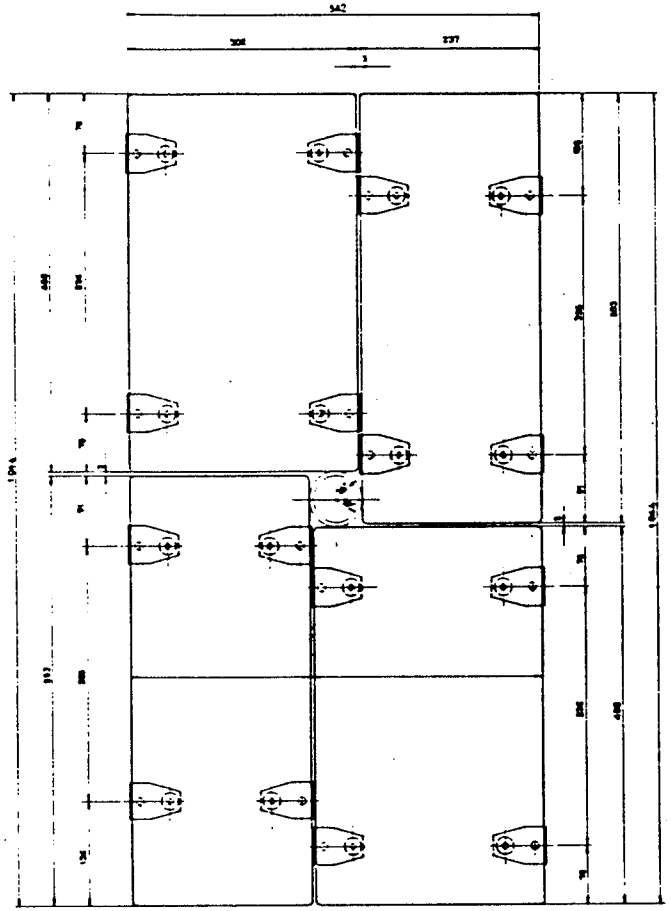

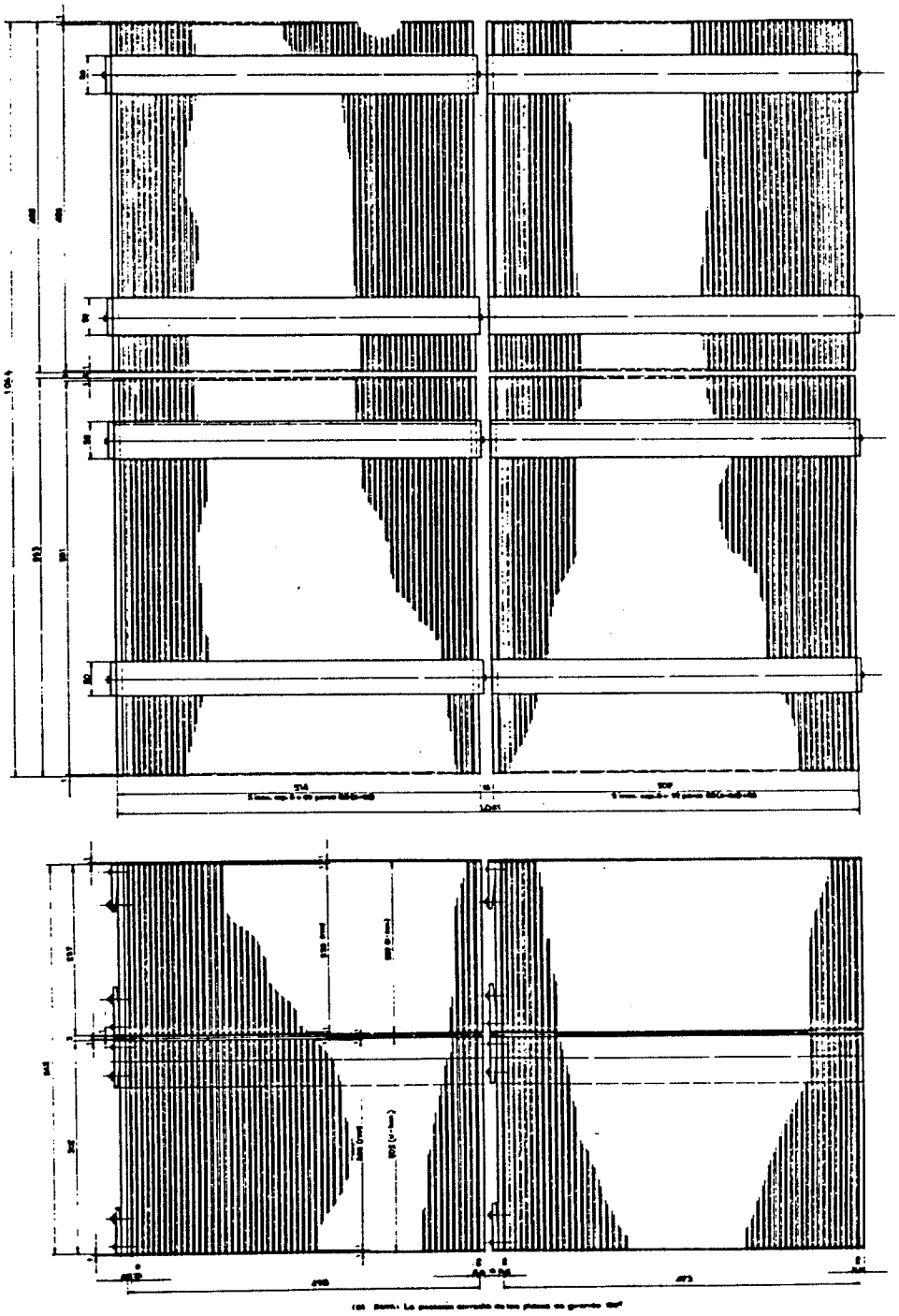

Fig. 4

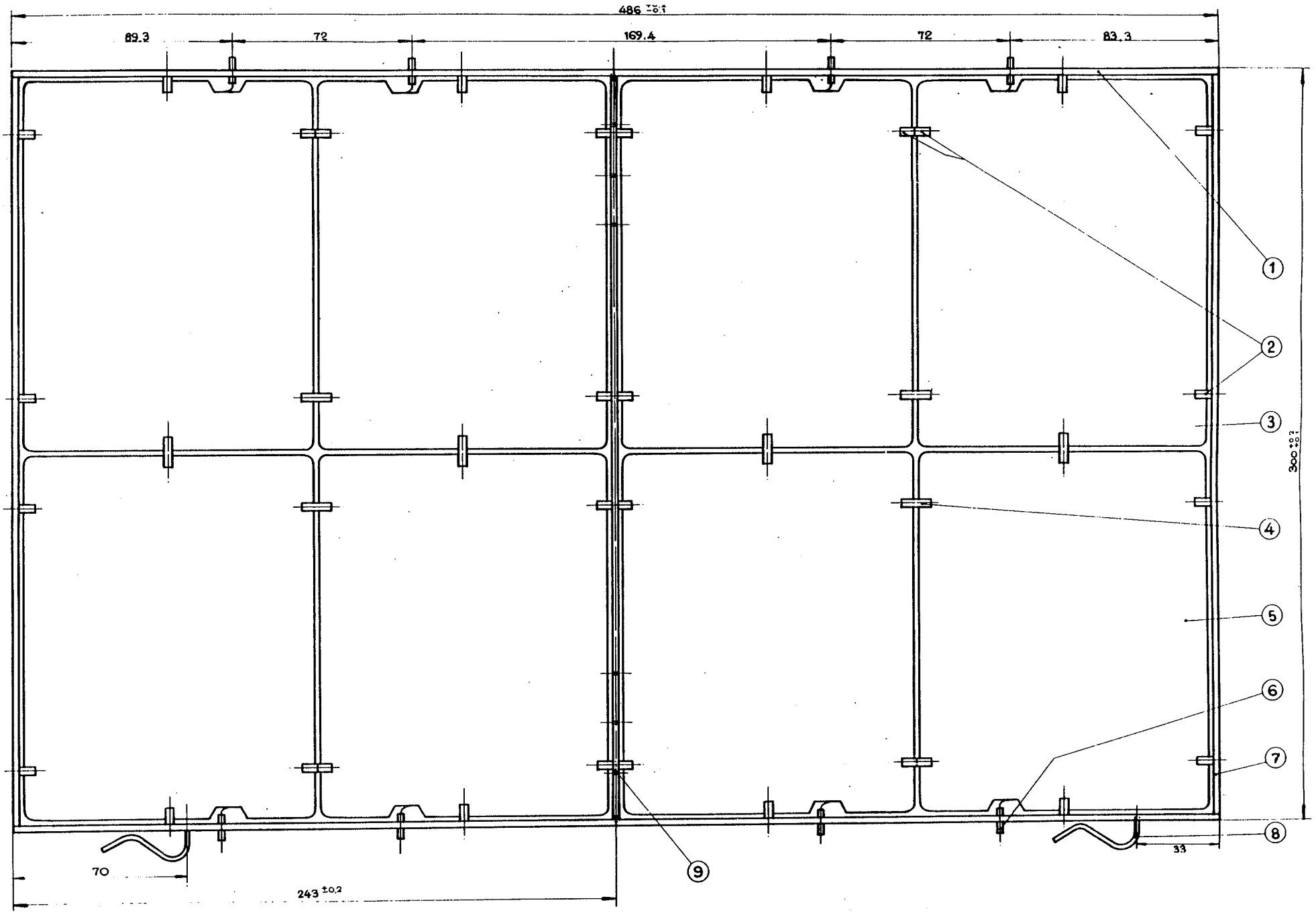

Fig. 5

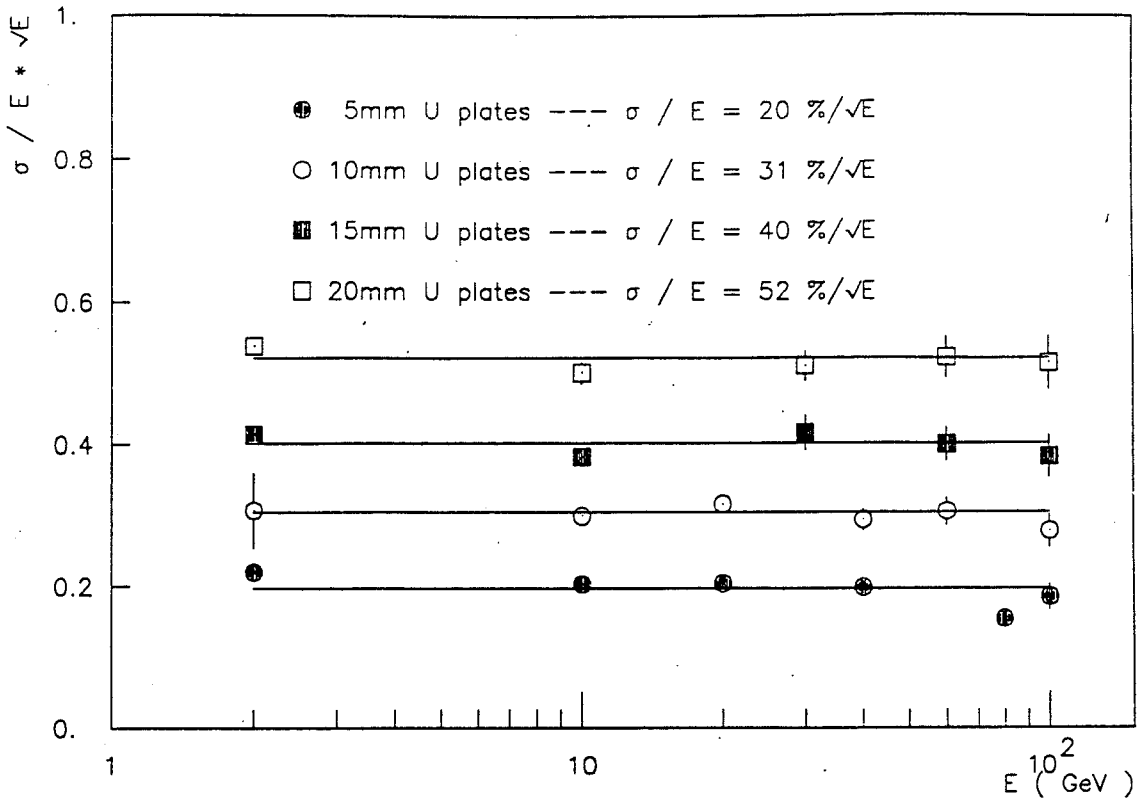
σ / E * √E
1.
0.8
0.6
0.4
0.2
0.
5mm U plates --- σ / E = 20 %/√E
10mm U plates --- σ / E = 31 %/√E
15mm U plates --- σ / E = 40 %/√E
20mm U plates --- σ / E = 52 %/√E
1
10
10^2
E (GeV)

Fig. 6(a)

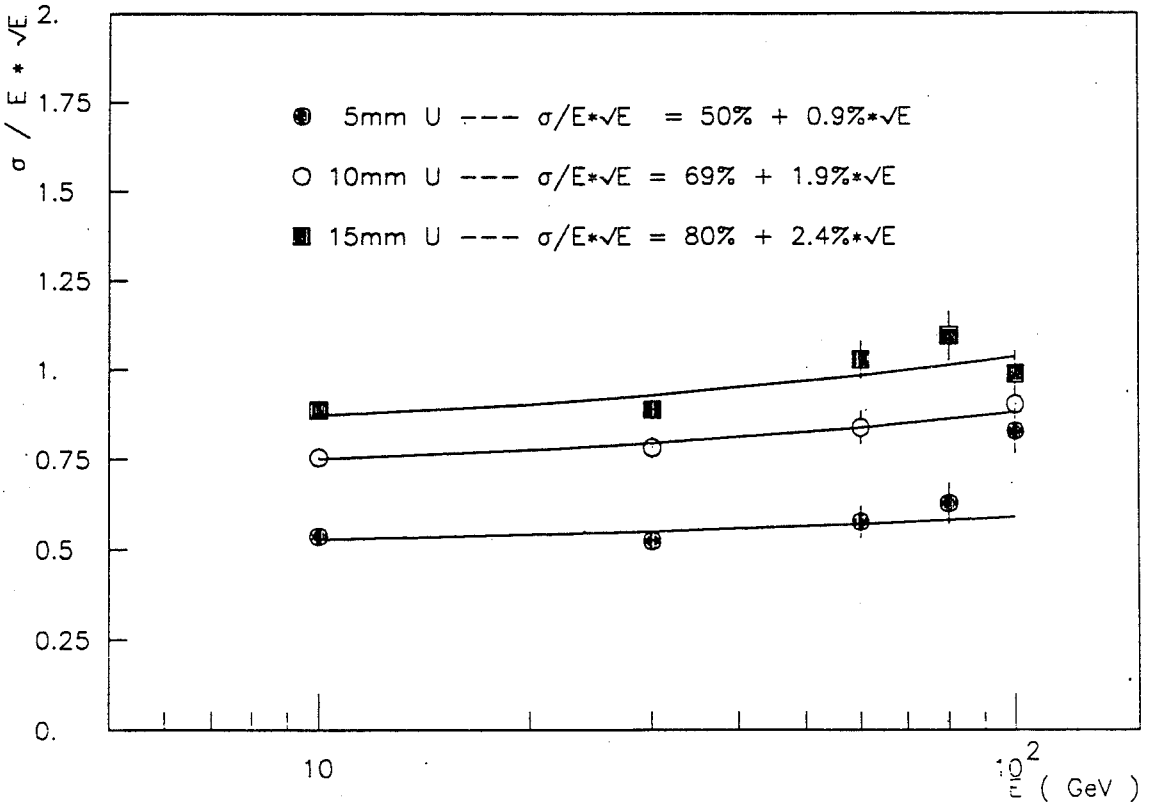
σ / E * √E
2.
1.75
1.5
1.25
1.
0.75
0.5
0.25
0.
5mm U --- σ/E*√E = 50% + 0.9%*√E
10mm U --- σ/E*√E = 69% + 1.9%*√E
15mm U --- σ/E*√E = 80% + 2.4%*√E
10
10^2
E (GeV)

Fig. 6(b)

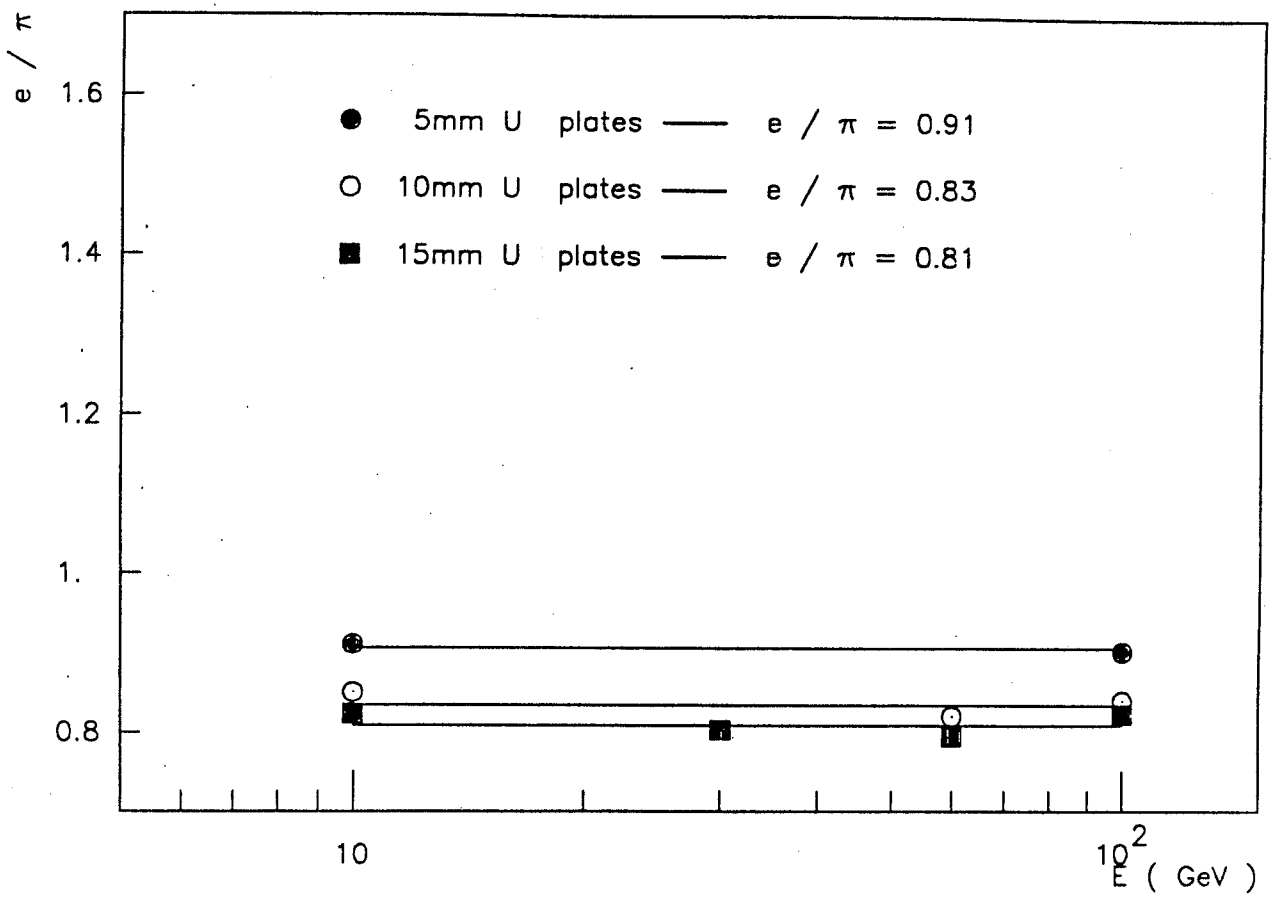
e / π
1.6
1.4
1.2
1.
0.8
5mm U plates —— e / π = 0.91
10mm U plates —— e / π = 0.83
15mm U plates —— e / π = 0.81
10
10^2
E (GeV)

Fig. 7

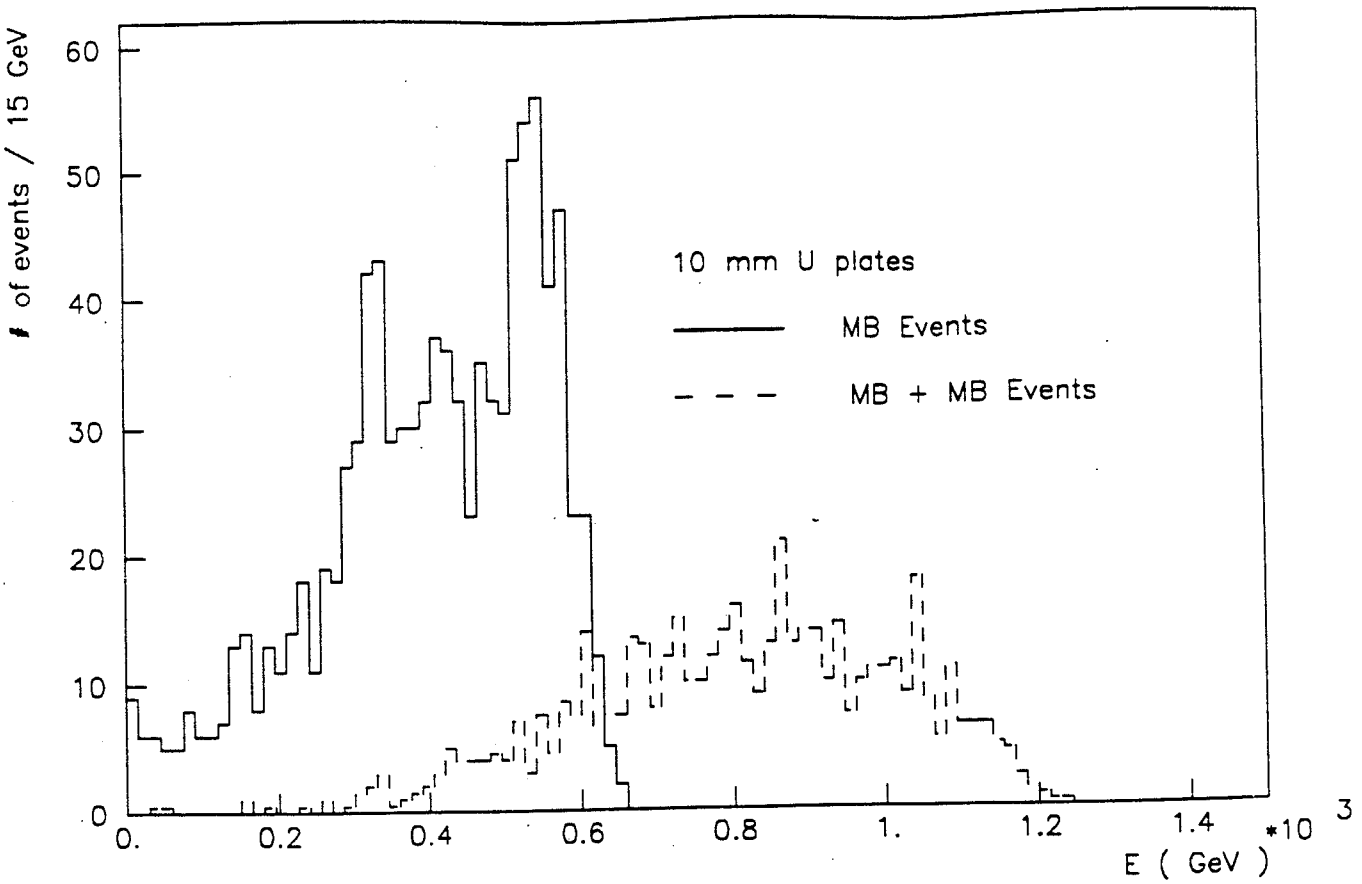
# of events / 15 GeV
60
50
40
30
20
10
0
0.
0.2
0.4
0.6
0.8
1.
1.2
1.4
*10 3
E (GeV)
10 mm U plates
MB Events
MB + MB Events

Fig. 8(a)

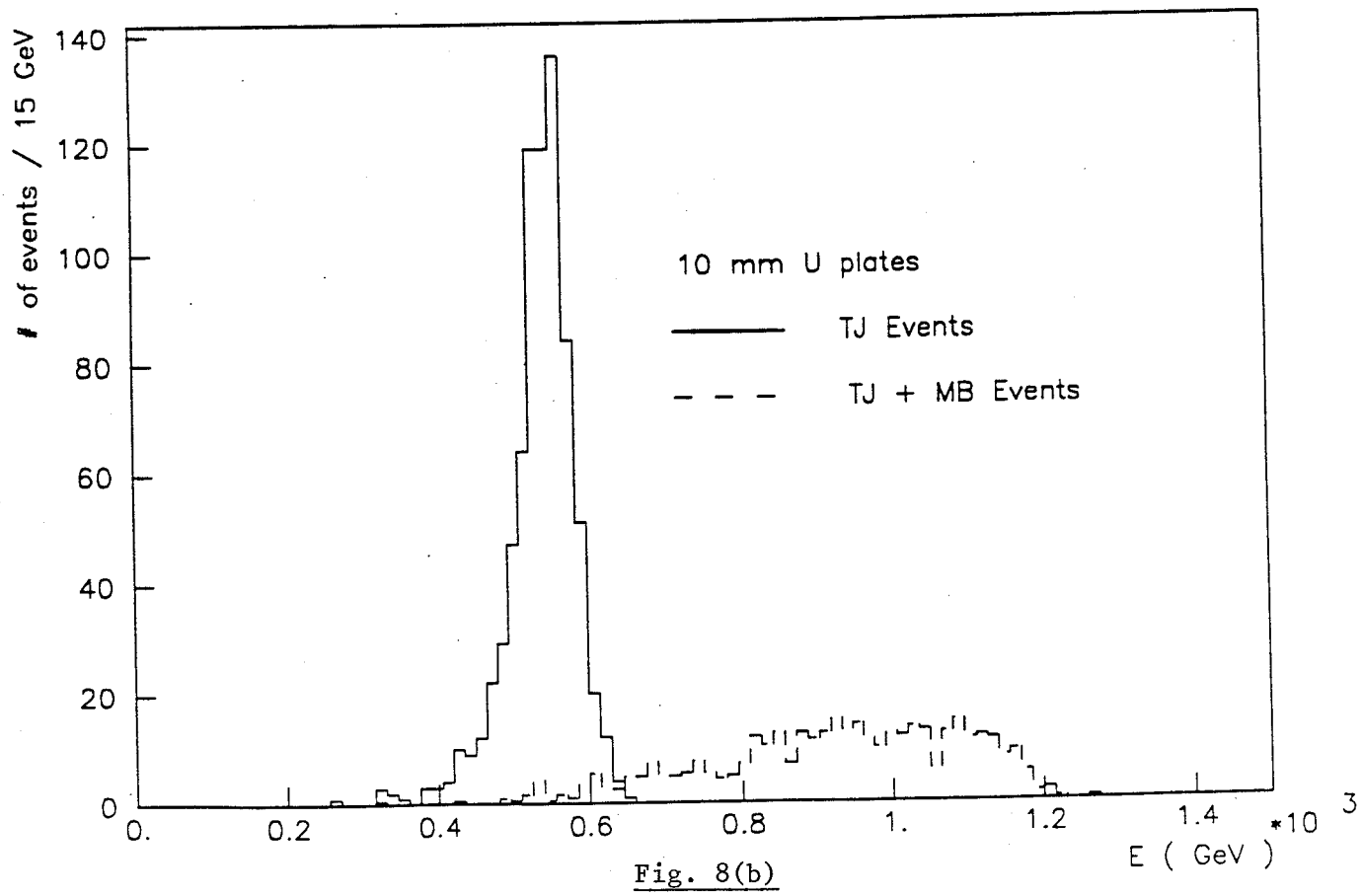
# of events / 15 GeV
140
120
100
80
60
40
20
0
0.
0.2
0.4
0.6
0.8
1.
1.2
1.4
*10 3
E (GeV)
10 mm U plates
TJ Events
TJ + MB Events

Fig. 8(b)

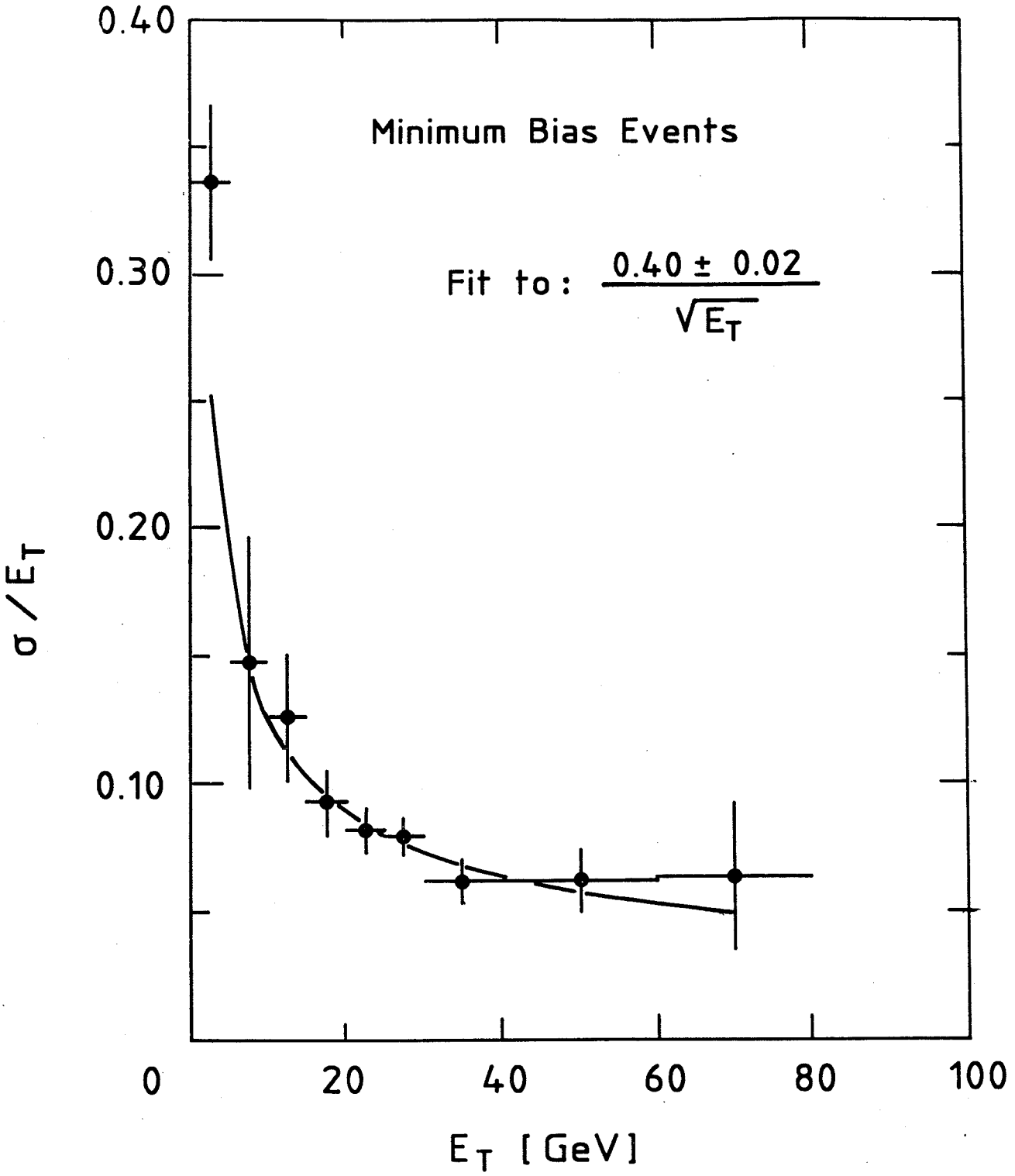
0.40
0.30
0.20
0.10
0
20
40
60
80
100
Minimum Bias Events
Fit to: $\frac{0.40 \pm 0.02}{\sqrt{E_T}}$
σ / E_T
E_T [GeV]

Fig. 9

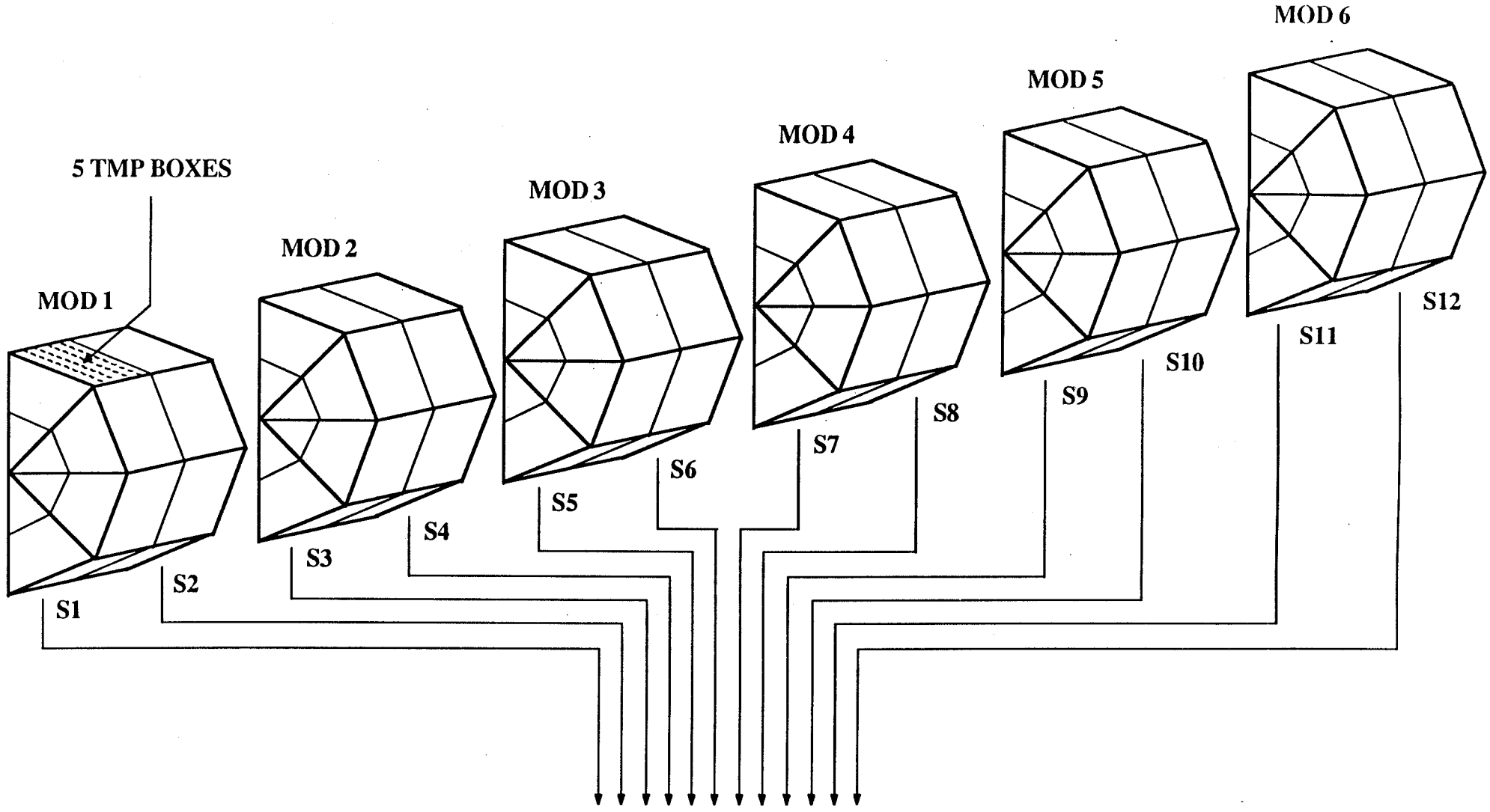
MOD 6
MOD 5
MOD 4
5 TMP BOXES
MOD 3
MOD 2
MOD 1
S12
S11
S10
S9
S8
S7
S6
S5
S4
S3
S2
S1
8 R - Φ ELECTRODES x 12 SAMPLINGS

Fig. 10